

Body Fat Estimation from Surface Meshes using Graph Neural Networks

Tamara T. Mueller^{*1,2}, Siyu Zhou^{*1}, Sophie Starck¹, Friederike Jungmann²,
Alexander Ziller^{1,2}, Orhun Aksoy¹, Danylo Movchan¹, Rickmer Braren²,
Georgios Kaissis^{1,2,4}, and Daniel Rueckert^{1,3}

¹ Institute for AI in Medicine and Healthcare, Faculty of Informatics, Technical University of Munich

² Department of Diagnostic and Interventional Radiology, Faculty of Medicine, Technical University of Munich

³ Department of Computing, Imperial College London

⁴ Institute for Machine Learning in Biomedical Imaging, Helmholtz-Zentrum Munich
tamara.mueller@tum.de

Abstract. Body fat volume and distribution can be a strong indication for a person’s overall health and the risk for developing diseases like type 2 diabetes and cardiovascular diseases. Frequently used measures for fat estimation are the body mass index (BMI), waist circumference, or the waist-hip-ratio. However, those are rather imprecise measures that do not allow for a discrimination between different types of fat or between fat and muscle tissue. The estimation of visceral (VAT) and abdominal subcutaneous (ASAT) adipose tissue volume has shown to be a more accurate measure for named risk factors. In this work, we show that triangulated body surface meshes can be used to accurately predict VAT and ASAT volumes using graph neural networks. Our methods achieve high performance while reducing training time and required resources compared to state-of-the-art convolutional neural networks in this area. We furthermore envision this method to be applicable to cheaper and easily accessible medical surface scans instead of expensive medical images.

1 Introduction

The estimation of body composition measures refers to the qualification and quantification of different tissue types in the body as well as the estimation of their distribution throughout the body. These measures can function as risk factors of individuals and be an indicator for health and mortality risk [1,12]. One component of body composition analysis is the estimation of fatty tissue volume in the body. The strong correlation between body composition and disease risk has led to a routine examination of measures indicating body composition in medical exams. The body mass index (BMI), for example, measures the ratio between a person’s weight and height and has been shown to be an indicator for developing cardiovascular diseases, type 2 diabetes, as well as overall mortality

* These authors contributed equally to this work.

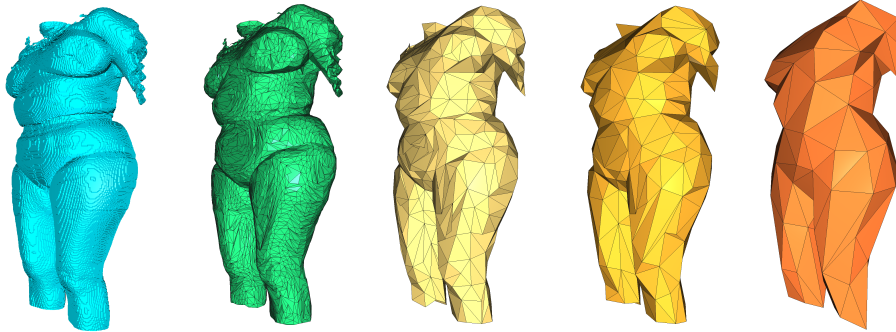


Fig. 1. Visualisation of body surface meshes at different decimation rates; The most left mesh shows the original mesh, then left to right are visualisations of decimated meshes with ten thousand, one thousand, five hundred and two hundred faces.

[28,12,3,32]. Additionally, the waist circumference and waist-hip-ratio can be used as an indication for body fat distribution [42,48,25,6]. These metrics are easy, fast, and cheap to assess. However, they have strong limitations. They are imprecise as they do not allow for a more accurate assessment of the distribution of body fat or to differentiate between weight that stems from muscle or fat tissue. Understanding the specific differences between different types of fatty tissue and their impact on health risks is crucial for accurately assessing an individual’s risk factors and enabling personalised medical care. Towards this goal, several works have investigated methods to identify variations of fat distribution in the body and the quantification of fatty tissues [54,29].

Body fat can be divided into different types of fat. Two commonly investigated types are *visceral fat* (VAT), which surrounds the abdominal organs, and *abdominal subcutaneous fat* (ASAT), which is located beneath the skin. Studies have shown that especially visceral fat can have a negative impact on a person’s health [40,8,47]. Therefore, a separate analysis of VAT and ASAT is an important step towards gaining accurate insights into body composition. Several works have investigated a precise estimation of VAT and ASAT volumes from medical images, like magnetic resonance (MR) [29] and computed tomography (CT) images [23], dual-energy X-ray absorptiometry (DXA) assessment [41], or ultrasound imaging [7]. Deep learning techniques have shown promising results in analysing these medical images in order to estimate body composition values [29,23,53,43].

In this work, we perform VAT and ASAT volume prediction from full body triangulated surface meshes using graph neural networks (GNNs). We show that GNNs allow to utilise the full 3D data at hand, thereby achieving better results than state-of-the-art convolutional neural networks (CNNs) on 2D silhouettes, while requiring significantly less training time and therefore resources. Both ours and related work, such as [29], use data extracted from MR images. However,

MR imaging is a very expensive technique, which is highly unequally distributed around the globe. The access to MR scanners in lower income countries is much more limited [18]. Furthermore, the acquisition of MR images is time consuming and very unlikely to be used for routine exams. Given the light computational weight and fast nature of our method, we envision it to be applied to data acquired from much simpler surface scans in the future and enable an incorporation into routine medical examination.

2 Background and Related Work

In the following, we summarise related works on body fat estimation from medical (and non-medical) images, define triangulated meshes and the concept of graph neural networks and show some of their application to medical data, with a focus on surface meshes.

2.1 Body Fat Estimation from Medical Imaging

Body fat estimation has been part of routine medical assessments for decades through the analysis of simple measurements such as BMI or waist circumference [17]. However, more elaborate ways such as using proxy variables derived from medical images, like dual energy X-ray absorptiometry (DXA), CT or MR images, have achieved more accurate results. Multiple studies have successfully assessed patient body composition based upon DXA [22,15,41]. Hemke et al. [23] and Nowak et al. [43] show successful utilisation of CT images for body composition assessment. Works like [31] use segmentation algorithms to identify fatty tissue in MR scans, from which body composition values can be derived. Tian et al. [50] estimate body composition measures based on 2D photography, not even requiring medical imaging techniques. Many of these approaches focus on predicting specific types of adipose tissue [36,39,29,31]. One idea, that has been followed by several works is the utilisation of silhouettes, a binary 2D projection of the outline of the body extracted from images. Xie et al. [54] use silhouettes generated from DXA whole-body scans to estimate shape variations and Klarqvist et al. [29] use silhouettes derived from MR Images for VAT and ASAT volume estimation using CNNs. The latter use two-dimensional coronal and sagittal silhouettes of the body outline and predict VAT and ASAT volume using convolutional neural networks. The silhouettes are extracted from the full-body magnetic resonance (MR) scans of the UK Biobank dataset [49]. In our work, we propose to switch from full medical images or binary silhouettes to surface meshes for fat volume prediction, which allows to integrate the full potential of the 3D surface into deep learning methods, while using the light-weight and fast method of graph neural networks (GNNs).

2.2 Triangulated Meshes

In this work, we use triangulated surface meshes of the body outline. A mesh structure can be interpreted as a specific 3D representation of a graph. A graph

$G := (V, E)$ is defined by a set of nodes V and a set of edges E , connecting pairs of nodes. The nodes usually contain node features, which can be summarised in a node features matrix \mathbf{X} . A triangulated mesh M has the same structure, commonly holding the 3D coordinates of the nodes as node features. All edges form triangular faces that define the surface of the object of interest –in our case: body surfaces. A visualisation of such meshes can be found in Figure 1.

2.3 Graph Neural Networks

Graph neural networks have opened the field of deep learning to non-Euclidean data structures such as graphs and meshes [11]. Since their introduction by [20] and [46], they have been utilised in various domains, including medical research [2,14]. Graphs are, for example, frequently used for representations of brain graphs [9], research in drug discovery [10], or bioinformatics [55,56]. One native data structure that benefits from the utilisation of graph neural networks are surface meshes [11]. GNNs on mesh datasets have also advanced research in the medical domain such as brain morphology estimation [5], which can be used for Alzheimer’s disease classification, or for the predicting of soft tissue deformation in image-guided neurosurgery [45].

In general, GNNs follow a so-called message passing scheme, where node features are aggregated among neighbourhoods, following the underlying graph structure [27,13,24,30]. This way, after each iteration, a new embedding for the node features is learned. In this work, we use Graph SAGE [21] convolutions, which were designed for applications on large graphs. The mean aggregator architecture for a node $v \in \mathcal{V}$ at step k is defined as follows:

$$h_v^k = \sigma(\mathbf{W} \cdot \text{MEAN}(\{h_v^{k-1}\} \cup \{h_u^{k-1}, \forall u \in \mathcal{N}_v\})). \quad (1)$$

\mathcal{N}_v is the neighbourhood of node v , \mathbf{W} is a learnable weight matrix, and MEAN the mean aggregator, which combines the node features of v at the previous step and the node features of v ’s neighbours.

3 Methods

We construct three different model architectures: (a) a graph neural network, (b) a simple convolutional neural network (CNN), and (c) a DenseNet and compare their performance. All models are trained using the Adam optimiser [26] and Shrinkage loss [38] and all results reported are cross-validated based on a 5-fold data split. We use a Quadro RTX 8000 GPU for our experiments and all models predict both targets –VAT and ASAT– with the same network, following the approach from [29].

GNN Architecture We perform a whole-graph regression task on the input meshes. The model architecture consists of a three-layer GNN with SAGE graph convolutions [21] and batch normalisation layers, followed by a max aggregation

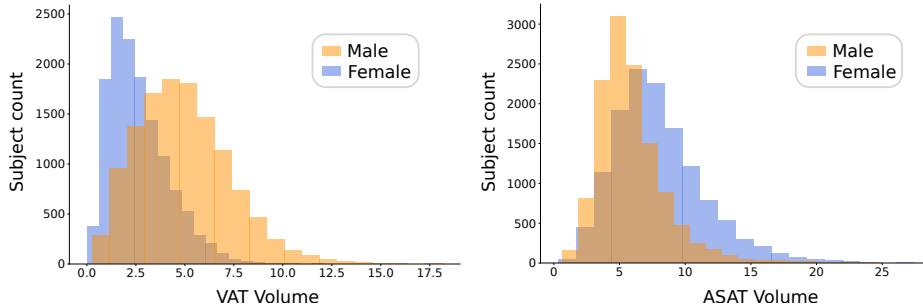


Fig. 2. Distribution of VAT (left) and ASAT (right) volume of male and female subjects in the cohort. Male subjects tend to have more VAT volume, whereas female subjects tend to have more ASAT volume.

and a three-layer multi-layer perceptron (MLP). Hyperparameters such as learning rate and GNN layers are selected by manual tuning. All GNNs are trained for 150 epochs.

CNN Architecture In order to compare our results to the work by Klarqvist et al. [29], we also train a DenseNet and a simpler CNN on the silhouette data. DenseNet is a CNN which is more densely connected, where each layer takes all previous outputs as an input. For our DenseNet implementation, we follow the architecture in [29]. We additionally construct a simpler CNN architecture that consists of three 2D convolutions, followed by a three-layer MLP, matching the design of the graph neural networks. Both convolutional networks are trained for 20 epochs on a 2D input image, that consist of a sagittal and a coronal view of the binary silhouette masks of the MR images, following the pipeline in [29].

4 Experiments and Results

We use a subset of the UK Biobank dataset [49], which is a large-scale medical database. It contains a variety of imaging data, genetics, and life-style information from almost 65 000 subjects and was acquired in the United Kingdom. In this work, we use the neck-to-knee magnetic resonance images of a subset of 25 298 subjects, for which the labels are available (12 210 male and 13 088 female). The mean age of this cohort is 62.95 years. The VAT and ASAT distributions of male and female subjects are visualised in Figure 2. We can see that female subjects tend to have a higher ASAT volume, whereas male subjects tend to have more VAT. As labels, we used the reported VAT and ASAT volumes in the UK Biobank (field IDs: 22407 and 22408).

4.1 Data Processing

The experiments in this work are performed on triangulated body surface meshes that are extracted from the neck-to-knee MR images from the UK Biobank

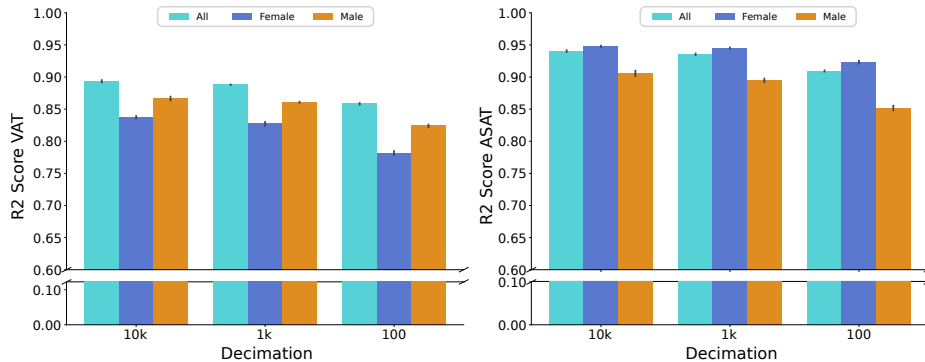


Fig. 3. R2 score results of VAT (left) and ASAT (right) predictions for all subjects, only males, and only females.

[44]. These were acquired in stations and merged through stitching [33]. In order to extract the surface meshes, we first perform an algorithmic whole-body segmentation by a succession of morphological operations on the stitched MR scans. We then convert these segmentations into surface meshes using the marching cubes algorithm [37] and the open3d library [57]. In order to investigate how much the surface meshes can be simplified, we decimate them into meshes consisting of different numbers of faces. We use meshes with 10 000, 5 000, 1 000, 500, 200, and 100 faces. The number of nodes is always half the number of faces, following Euler’s formula for triangular meshes [16]. Subsequently, the meshes are registered into a common coordinate system, using the iterative closest point algorithm [4]. As a reference subject, the most average subject in the dataset was selected based on height, weight, and age. The resulting decimated and registered surface meshes are then used for graph learning. Figure 1 shows an example of a body surface mesh at different decimation rates.

4.2 Results

Table 1 summarises the results of the GNNs and CNNs for ASAT and VAT volume prediction. We report the 5-fold cross-validation results on the test set of the best performing models, evaluated on the validation loss. We compare the results of our graph neural networks (GNNs) with the results achieved by the DenseNet from [29] and the results of a simpler CNN (which we call *CNN* in the tables). We furthermore report the training times of all models, measured by the full training process for 150 and 20 epochs for GNNs and CNNs, respectively. All GNNs are trained on the body surface meshes, whereas the CNNs are trained on the silhouettes, following the approach proposed in [29]. We evaluate the GNNs on body surface meshes at different decimation rates of ten thousand, five thousand, one thousand, 500, 200, and 100 faces per mesh (see Figure 1 for a visualisation of some of these decimated meshes). The best test performances are highlighted in bold, so are the shortest training times. We can see that the

Table 1. Results for VAT and ASAT volume estimation; We report the R2 scores on the test set with standard deviations based on 5-fold cross validation, as well as the training times of the full training in minutes.

Tissue	Model	Decim.	Test R2	Time (min)	
VAT	GNN (ours)	100	0.858 ± 0.001	8.36	
		200	0.872 ± 0.001	8.63	
		500	0.882 ± 0.001	9.01	
		1k	0.888 ± 0.001	10.11	
		5k	0.893 ± 0.002	22.36	
		10k	0.893 ± 0.003	37.75	
		CNN (ours)	-	0.874 ± 0.001	16.20
	DenseNet	-	0.878 ± 0.004	95.79	
	ASAT	GNN (ours)	100	0.909 ± 0.001	8.36
			200	0.921 ± 0.002	8.63
500			0.931 ± 0.001	9.01	
1k			0.935 ± 0.002	10.11	
5k			0.938 ± 0.000	22.36	
10k			0.941 ± 0.002	37.75	
CNN (ours)			-	0.921 ± 0.002	16.20
DenseNet		-	0.934 ± 0.002	95.79	

simpler CNN architecture almost matches performance of the DenseNet proposed by [29], while requiring less training time. The GNNs outperform the CNN and the DenseNet, when the utilised meshes are not heavily decimated. But even highly decimated surface meshes with one hundred faces, only result in minor performance loss while requiring less than ten times less training time compared to the DenseNet. We envision the utilisation of the surface meshes and graph neural networks to allow for more efficient model training and the utilisation of the full 3D structure of the body, while keeping resource requirements low.

Male and female subjects show different distributions in VAT and ASAT volume. While male subjects tend to have more VAT, females tend to have more ASAT. Figure 2 shows the distributions of the fat volumes of the two sex groups. We therefore compare the results of our method for female and male subjects separately. Table 2 summarises the results of all GNNs and CNNs for VAT and ASAT volume prediction split by sex. The best performing model for each fat type and sex is highlighted in bold. We can see that the predictions of VAT volume tends to be better on male subjects whereas the prediction of ASAT volume achieves slightly higher scores for the female subject. The GNNs, however, seem to show a slightly lower gap in performance between the sex groups. We attribute the difference in performance on the different fatty tissue types to the varying distributions in fat volume between the sex groups.

Table 2. Results of VAT and ASAT volume prediction split by subject sex; all reported values are R2 scores on the test set, cross-validated across 5 folds.

Fat tissue	Model	Decimation	Female R2	Male R2
VAT	GNN (ours)	100	0.782 ± 0.004	0.824 ± 0.003
		200	0.804 ± 0.006	0.840 ± 0.003
		500	0.815 ± 0.008	0.854 ± 0.003
		1k	0.827 ± 0.004	0.861 ± 0.001
		5k	0.831 ± 0.006	0.868 ± 0.002
		10k	0.837 ± 0.002	0.867 ± 0.004
	CNN (ours)	-	0.804 ± 0.003	0.845 ± 0.002
	DenseNet	-	0.811 ± 0.006	0.849 ± 0.006
ASAT	GNN (ours)	100	0.923 ± 0.003	0.852 ± 0.004
		200	0.934 ± 0.001	0.870 ± 0.006
		500	0.940 ± 0.002	0.890 ± 0.002
		1k	0.945 ± 0.001	0.895 ± 0.004
		5k	0.945 ± 0.000	0.903 ± 0.002
		10k	0.948 ± 0.001	0.906 ± 0.005
	CNN (ours)	-	0.934 ± 0.002	0.870 ± 0.002
	DenseNet	-	0.944 ± 0.001	0.891 ± 0.003

5 Discussion and Conclusion

In this work, we introduce a graph neural network-based method that enables adipose tissue volume prediction for visceral (VAT) and abdominal subcutaneous (ASAT) fat from triangulated surface meshes. The assessment of fatty tissue has high clinical relevance, since it has been shown to be a strong risk factor for diseases like type 2 diabetes and cardiovascular diseases [28,32]. Especially a separate estimation of the two different fat tissues VAT and ASAT has shown to be a relevant medical assessment, since VAT is known to have a higher correlation with disease development compared to ASAT [40,8,47]. We here use graph neural networks and triangulated surface meshes, extracted from full-body MR scans and show that they achieve accurate VAT and ASAT volume predictions. We investigate how different decimation rates impact model performance and training times. Figure 4 visualises this correlation. The bars in the left figure show the average ASAT volume prediction R2 scores on the test set of the GNNs trained on the differently decimated meshes. The overlaid line plot notes the corresponding training times. We can see that at one thousand faces, we reach an optimal trade-off between training time and performance. Training the GNN on the meshes with one thousand faces only takes about 10 minutes and achieves high results of 0.893 R2 on VAT and 0.935 on ASAT volume prediction. On the right in Figure 4, we visualise the linear relation between the training time and the number of faces in the meshes. Training time also corresponds linearly to energy consumption in kWh. We attribute the comparably high performance of the

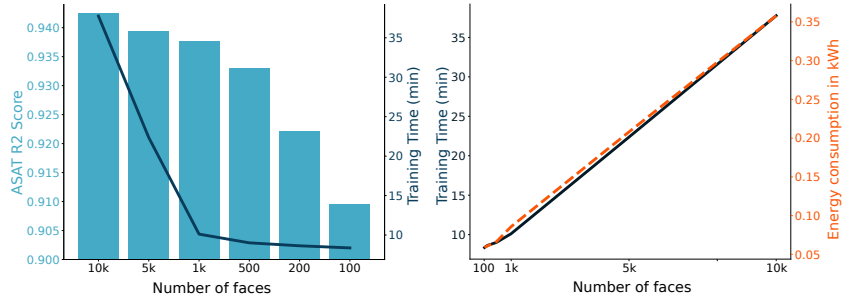


Fig. 4. Relationship between training time and decimation rate of the meshes; The left plot shows the ASAT R2 scores (bars) and the corresponding training time, the right plot shows the linear relation between the training time or the energy consumption in kWh and the number of faces of the meshes.

strongly decimated meshes to the fact that the most outer coordinates/nodes still remain in the meshes, which carry a lot of information about the outline of a body.

The light-weight nature of GNNs allows for the usage of the full 3D data, while significantly reducing resource requirements and run time compared to 3D image-based methods. This shows great promise in the effort of bridging the gap between cheap, fast, but imprecise measures –such as BMI and waist circumference– and time-consuming, costly, but accurate methods such as medical imaging (CT, MR, or DXA).

6 Limitations and Future Work

We see high potential in the utilisation of surface meshes and graph neural networks, given that the full 3D data can be utilised compared to only using binary silhouette projections like in [29]. The low training times as well as the high scores of the GNNs show the successful application to fat volume prediction. We note that we compare the run time of the training loops only. This does not include any pre-processing that is required for both silhouette-based and surface mesh-based approaches. The GNN architecture is based on SAGE graph convolutions [21], because they achieved the best results in our experiments, compared to graph attention networks [51] and graph convolutional networks [27]. A potential improvement of our method would be the utilisation of other mesh-specific convolutions such as adaptive graph convolution pooling [19] or FeaStNet [52]. Another interesting direction to explore is the utilisation of deeper GNNs. Li et al. [34], for example, introduce a method that enables the utilisation of deeper GNNs without over-smoothing –a commonly known problem with GNNs. Over-smoothing refers to the issue that deep GNNs do not achieve high performance because all node embeddings in the graph converge to the same value [35].

Our experiments are performed on surface meshes, that were extracted from MR images. However, we envision this method to work equally well on designated surface scans, without requiring expensive and time-consuming MR scans. We intend to investigate this in future work and apply our method to surface scans, which are for example acquired for dermatological examinations. This would eliminate the need for expensive MR scans and could lead to an embedding of this technique into routine medical examination.

Acknowledgements TM and SS were supported by the ERC (Deep4MI - 884622). This work has been conducted under the UK Biobank application 87802. SS has furthermore been supported by BMBF and the NextGenerationEU of the European Union.

References

1. Afshin, A., Reitsma, M.B., Murray, C.J.: Health effects of overweight and obesity in 195 countries. *The New England journal of medicine* **377**(15), 1496–1497 (2017)
2. Ahméd-Aristizabal, D., Armin, M.A., Denman, S., Fookes, C., Petersson, L.: Graph-based deep learning for medical diagnosis and analysis: past, present and future. *Sensors* **21**(14), 4758 (2021)
3. Anderson, M.R., Geleris, J., Anderson, D.R., Zucker, J., Nobel, Y.R., Freedberg, D., Small-Saunders, J., Rajagopalan, K.N., Greendyk, R., Chae, S.R., et al.: Body mass index and risk for intubation or death in sars-cov-2 infection: a retrospective cohort study. *Annals of internal medicine* **173**(10), 782–790 (2020)
4. Arun, K.S., Huang, T.S., Blostein, S.D.: Least-squares fitting of two 3-d point sets. *IEEE Transactions on Pattern Analysis and Machine Intelligence* **PAMI-9**(5), 698–700 (1987). <https://doi.org/10.1109/TPAMI.1987.4767965>
5. Azcona, E.A., Besson, P., Wu, Y., Punjabi, A., Martersteck, A., Dravid, A., Parrish, T.B., Bandt, S.K., Katsaggelos, A.K.: Interpretation of brain morphology in association to alzheimer’s disease dementia classification using graph convolutional networks on triangulated meshes. In: *Shape in Medical Imaging: International Workshop, ShapeMI 2020, Held in Conjunction with MICCAI 2020, Lima, Peru, October 4, 2020, Proceedings*. pp. 95–107. Springer (2020)
6. Baioumi, A.Y.A.A.: Comparing measures of obesity: waist circumference, waist-hip, and waist-height ratios. In: *Nutrition in the Prevention and Treatment of Abdominal Obesity*, pp. 29–40. Elsevier (2019)
7. Bazzocchi, A., Filonzi, G., Ponti, F., Albisinni, U., Guglielmi, G., Battista, G.: Ultrasound: Which role in body composition? *European Journal of Radiology* **85**(8), 1469–1480 (2016)
8. Bergman, R.N., Kim, S.P., Catalano, K.J., Hsu, I.R., Chiu, J.D., Kabir, M., Hucking, K., Ader, M.: Why visceral fat is bad: mechanisms of the metabolic syndrome. *Obesity* **14**(2S), 16S (2006)
9. Bessadok, A., Mahjoub, M.A., Rekik, I.: Graph neural networks in network neuroscience. *IEEE Trans. on Pattern Analysis and Machine Intelligence* (2022)
10. Bonner, S., Barrett, I.P., Ye, C., Swiers, R., Engkvist, O., Bender, A., Hoyt, C.T., Hamilton, W.L.: A review of biomedical datasets relating to drug discovery: a knowledge graph perspective. *Briefings in Bioinformatics* **23**(6) (2022)

11. Bronstein, M.M., Bruna, J., LeCun, Y., Szlam, A., Vandergheynst, P.: Geometric deep learning: going beyond euclidean data. *IEEE Signal Processing Magazine* **34**(4), 18–42 (2017)
12. Calle, E.E., Rodriguez, C., Walker-Thurmond, K., Thun, M.J.: Overweight, obesity, and mortality from cancer in a prospectively studied cohort of us adults. *New England Journal of Medicine* **348**(17), 1625–1638 (2003)
13. Chiang, W.L., Liu, X., Si, S., Li, Y., Bengio, S., Hsieh, C.J.: Cluster-gcn: An efficient algorithm for training deep and large graph convolutional networks. In: *Proceedings of the 25th ACM SIGKDD international conference on knowledge discovery & data mining*. pp. 257–266 (2019)
14. Ding, K., Zhou, M., Wang, Z., Liu, Q., Arnold, C.W., Zhang, S., Metaxas, D.N.: Graph convolutional networks for multi-modality medical imaging: Methods, architectures, and clinical applications. *arXiv:2202.08916* (2022)
15. Direk, K., Cecelja, M., Astle, W., Chowienczyk, P., Spector, T.D., Falchi, M., Andrew, T.: The relationship between dxa-based and anthropometric measures of visceral fat and morbidity in women. *BMC cardiovascular disorders* **13**, 1–13 (2013)
16. Euler, L.: De summis serierum reciprocarum. *Commentarii academiae scientiarum Petropolitanae* pp. 123–134 (1740)
17. Fan, Z., Chiong, R., Hu, Z., Keivanian, F., Chiong, F.: Body fat prediction through feature extraction based on anthropometric and laboratory measurements. *Plos one* **17**(2), e0263333 (2022)
18. Geethanath, S., Vaughan Jr, J.T.: Accessible magnetic resonance imaging: a review. *Journal of Magnetic Resonance Imaging* **49**(7), e65–e77 (2019)
19. Gopinath, K., Desrosiers, C., Lombaert, H.: Adaptive graph convolution pooling for brain surface analysis. In: Chung, A.C.S., Gee, J.C., Yushkevich, P.A., Bao, S. (eds.) *Information Processing in Medical Imaging*. pp. 86–98. Springer International Publishing, Cham (2019)
20. Gori, M., Monfardini, G., Scarselli, F.: A new model for learning in graph domains. In: *Proc. 2005 IEEE Int. joint conf. on neural networks*. vol. 2(2005), pp. 729–734 (2005)
21. Hamilton, W., Ying, Z., Leskovec, J.: Inductive representation learning on large graphs. *Advances in neural information processing systems* **30** (2017)
22. Harty, P.S., Sieglinger, B., Heymsfield, S.B., Shepherd, J.A., Bruner, D., Stratton, M.T., Tinsley, G.M.: Novel body fat estimation using machine learning and 3-dimensional optical imaging. *European journal of clinical nutrition* **74**(5), 842–845 (2020)
23. Hemke, R., Buckless, C.G., Tsao, A., Wang, B., Torriani, M.: Deep learning for automated segmentation of pelvic muscles, fat, and bone from ct studies for body composition assessment. *Skeletal radiology* **49**, 387–395 (2020)
24. Huang, Q., He, H., Singh, A., Lim, S.N., Benson, A.R.: Combining label propagation and simple models out-performs graph neural networks. *arXiv preprint arXiv:2010.13993* (2020)
25. Jacobs, E.J., Newton, C.C., Wang, Y., Patel, A.V., McCullough, M.L., Campbell, P.T., Thun, M.J., Gapstur, S.M.: Waist circumference and all-cause mortality in a large us cohort. *Archives of internal medicine* **170**(15), 1293–1301 (2010)
26. Kingma, D.P., Ba, J.: Adam: A method for stochastic optimization. *CoRR abs/1412.6980* (2014)
27. Kipf, T.N., Welling, M.: Semi-supervised classification with graph convolutional networks. *arXiv:1609.02907* (2016)

28. Kivimäki, M., Kuosma, E., Ferrie, J.E., Luukkonen, R., Nyberg, S.T., Alfredsson, L., Batty, G.D., Brunner, E.J., Fransson, E., Goldberg, M., et al.: Overweight, obesity, and risk of cardiometabolic multimorbidity: pooled analysis of individual-level data for 120 813 adults from 16 cohort studies from the usa and europe. *The Lancet Public Health* **2**(6), e277–e285 (2017)
29. Klarqvist, M.D., Agrawal, S., Diamant, N., Ellinor, P.T., Philippakis, A., Ng, K., Batra, P., Khera, A.V.: Silhouette images enable estimation of body fat distribution and associated cardiometabolic risk. *npj Digital Medicine* **5**(1), 105 (2022)
30. Kong, K., Li, G., Ding, M., Wu, Z., Zhu, C., Ghanem, B., Taylor, G., Goldstein, T.: Flag: Adversarial data augmentation for graph neural networks. arXiv preprint arXiv:2010.09891 (2020)
31. Küstner, T., Hepp, T., Fischer, M., Schwartz, M., Fritsche, A., Häring, H.U., Nikolaou, K., Bamberg, F., Yang, B., Schick, F., Gatidis, S., Machann, J.: Fully automated and standardized segmentation of adipose tissue compartments via deep learning in 3d whole-body mri of epidemiologic cohort studies. *Radiology. Artificial intelligence* **2** **6**, e200010 (2020)
32. Larsson, S.C., Bäck, M., Rees, J.M., Mason, A.M., Burgess, S.: Body mass index and body composition in relation to 14 cardiovascular conditions in uk biobank: a mendelian randomization study. *European heart journal* **41**(2), 221–226 (2020)
33. Lavdas, I., Glocker, B., Rueckert, D., Taylor, S., Aboagye, E., Rockall, A.: Machine learning in whole-body mri: experiences and challenges from an applied study using multicentre data. *Clinical radiology* **74**(5), 346–356 (2019)
34. Li, G., Muller, M., Thabet, A., Ghanem, B.: Deepgcns: Can gcns go as deep as cnns? In: Proceedings of the IEEE/CVF international conference on computer vision. pp. 9267–9276 (2019)
35. Li, Q., Han, Z., Wu, X.M.: Deeper insights into graph convolutional networks for semi-supervised learning. In: Proceedings of the AAAI conference on artificial intelligence. vol. 32 (2018)
36. Linder, N., Michel, S., Eggebrecht, T., Schaudinn, A., Blüher, M., Dietrich, A., Denecke, T., Busse, H.: Estimation of abdominal subcutaneous fat volume of obese adults from single-slice mri data – regression coefficients and agreement. *European Journal of Radiology* **130**, 109184 (2020). <https://doi.org/https://doi.org/10.1016/j.ejrad.2020.109184>, <https://www.sciencedirect.com/science/article/pii/S0720048X20303739>
37. Lorensen, W.E., Cline, H.E.: Marching cubes: A high resolution 3d surface construction algorithm. *Comput Graph* **21**, 163–169 (1987)
38. Lu, X., Ma, C., Ni, B., Yang, X., Reid, I., Yang, M.H.: Deep regression tracking with shrinkage loss. In: Proceedings of the European conference on computer vision (ECCV). pp. 353–369 (2018)
39. Lu, Y., Shan, Y., Dai, L., Jiang, X., Song, C., Chen, B., Zhang, J., Li, J., Zhang, Y., Xu, J., Li, T., Xiong, Z., Bai, Y., Huang, X.: Sex-specific equations to estimate body composition: Derivation and validation of diagnostic prediction models using uk biobank. *Clinical Nutrition* **42**(4), 511–518 (2023). <https://doi.org/https://doi.org/10.1016/j.clnu.2023.02.005>, <https://www.sciencedirect.com/science/article/pii/S0261561423000341>
40. Matsuzawa, Y., Nakamura, T., Shimomura, I., Kotani, K.: Visceral fat accumulation and cardiovascular disease. *Obesity research* **3**(S5), 645S–647S (1995)
41. Messina, C., Albano, D., Gitto, S., Tofanelli, L., Bazzocchi, A., Ulivieri, F.M., Guglielmi, G., Sconfienza, L.M.: Body composition with dual energy x-ray absorptiometry: from basics to new tools. *Quantitative imaging in medicine and surgery* **10**(8), 1687 (2020)

42. Neeland, I.J., Ross, R., Després, J.P., Matsuzawa, Y., Yamashita, S., Shai, I., Seidell, J., Magni, P., Santos, R.D., Arsenault, B., et al.: Visceral and ectopic fat, atherosclerosis, and cardiometabolic disease: a position statement. *The lancet Diabetes & endocrinology* **7**(9), 715–725 (2019)
43. Nowak, S., Faron, A., Luetkens, J.A., Geißler, H.L., Praktijnjo, M., Block, W., Thomas, D., Sprinkart, A.M.: Fully automated segmentation of connective tissue compartments for ct-based body composition analysis: a deep learning approach. *Investigative radiology* **55**(6), 357–366 (2020)
44. Petersen, S.E., Matthews, P.M., Bamberg, F., Bluemke, D.A., Francis, J.M., Friedrich, M.G., Leeson, P., Nagel, E., Plein, S., Rademakers, F.E., et al.: Imaging in population science: cardiovascular magnetic resonance in 100,000 participants of uk biobank-rationale, challenges and approaches. *Journal of Cardiovascular Magnetic Resonance* **15**(1), 1–10 (2013)
45. Salehi, Y., Giannacopoulos, D.: Physgmn: A physics-driven graph neural network based model for predicting soft tissue deformation in image-guided neurosurgery. *Advances in Neural Information Processing Systems* **35**, 37282–37296 (2022)
46. Scarselli, F., Gori, M., Tsoi, A.C., Hagenbuchner, M., Monfardini, G.: The graph neural network model. *IEEE trans. on neural networks* **20**(1), 61–80 (2008)
47. Shuster, A., Patlas, M., Pinthus, J., Mourtzakis, M.: The clinical importance of visceral adiposity: a critical review of methods for visceral adipose tissue analysis. *The British journal of radiology* **85**(1009), 1–10 (2012)
48. Song, X., Jousilahti, P., Stehouwer, C., Söderberg, S., Onat, A., Laatikainen, T., Yudkin, J., Dankner, R., Morris, R., Tuomilehto, J., et al.: Comparison of various surrogate obesity indicators as predictors of cardiovascular mortality in four european populations. *European Journal of Clinical Nutrition* **67**(12), 1298–1302 (2013)
49. Sudlow, C., Gallacher, J., Allen, N., Beral, V., Burton, P., Danesh, J., Downey, P., Elliott, P., Green, J., Landray, M., et al.: Uk biobank: an open access resource for identifying the causes of a wide range of complex diseases of middle and old age. *PLoS medicine* **12**(3), e1001779 (2015)
50. Tian, I.Y., Ng, B.K., Wong, M.C., Kennedy, S., Hwaung, P., Kelly, N., Liu, E., Garber, A.K., Curless, B., Heymsfield, S.B., et al.: Predicting 3d body shape and body composition from conventional 2d photography. *Medical Physics* **47**(12), 6232–6245 (2020)
51. Veličković, P., Cucurull, G., Casanova, A., Romero, A., Lio, P., Bengio, Y.: Graph attention networks. *arXiv preprint arXiv:1710.10903* (2017)
52. Verma, N., Boyer, E., Verbeek, J.: Feastnet: Feature-steered graph convolutions for 3d shape analysis. In: *Proceedings of the IEEE conference on computer vision and pattern recognition*. pp. 2598–2606 (2018)
53. Wang, B., Torriani, M.: Artificial intelligence in the evaluation of body composition. In: *Seminars in Musculoskeletal Radiology*. vol. 24, pp. 030–037. Thieme Medical Publishers (2020)
54. Xie, B., Avila, J.I., Ng, B.K., Fan, B., Loo, V., Gilsanz, V., Hangartner, T., Kalkwarf, H.J., Lappe, J., Oberfield, S., et al.: Accurate body composition measures from whole-body silhouettes. *Medical physics* **42**(8), 4668–4677 (2015)
55. Yi, H.C., You, Z.H., Huang, D.S., Kwok, C.K.: Graph representation learning in bioinformatics: trends, methods and applications. *Briefings in Bioinformatics* **23**(1), bbab340 (2022)
56. Zhang, X.M., Liang, L., Liu, L., Tang, M.J.: Graph neural networks and their current applications in bioinformatics. *Frontiers in genetics* **12**, 690049 (2021)

57. Zhou, Q.Y., Park, J., Koltun, V.: Open3D: A modern library for 3D data processing. arXiv:1801.09847 (2018)